

Polarized and unpolarized μ -pair meson-induced Drell–Yan production and the pion distribution amplitude

A. P. Bakulev*

Bogoliubov Laboratory of Theoretical Physics, JINR, 141980 Dubna, Russia

N. G. Stefanis†

Institut für Theoretische Physik II, Ruhr-Universität Bochum, D-44780 Bochum, Germany

O. V. Teryaev‡

*Bogoliubov Laboratory of Theoretical Physics,
JINR, 141980 Dubna, Russia*

(Dated: February 1, 2008)

Abstract

We present a detailed analysis of meson-induced massive lepton (muon) Drell–Yan production for the process $\pi^- N \rightarrow \mu^+ \mu^- X$, considering both an unpolarized nucleon target and longitudinally polarized protons. Using a QCD framework, we focus on the angular distribution of μ^+ , which is sensitive to the shape of the pion distribution amplitude, the goal being to test corresponding results against available experimental data. Predictions are made, employing various pion distribution amplitudes, for the azimuthal angle dependence of the μ^+ distribution in the polarized case, relevant for the planned COMPASS experiment. QCD evolution is given particular attention in both considered cases.

PACS numbers: 13.85.Qk, 12.38.Cy, 12.38.Bx, 13.88.+e

*Electronic address: bakulev@theor.jinr.ru

†Electronic address: stefanis@tp2.ruhr-uni-bochum.de

‡Electronic address: teryaev@theor.jinr.ru

I. INTRODUCTION

The meson-induced production of massive dileptons off baryons in the Drell–Yan (DY) process [1] $MB \rightarrow l^+l^-X$ provides a useful means of analyzing the quark structure of an unstable hadron, like the pion. Indeed, one can extract (see, for example, [2, 3]) in such a context the quark structure function of the pion and test the process independence of the nucleon structure function measured in deeply inelastic scattering.

On the other hand, for large Q^2 and large longitudinal momentum (carried by a pion’s quark constituent) the hadronic differential cross section for the production of a massive lepton pair via the annihilation of an antiquark and a quark in the colliding hadrons—pion and nucleon, respectively—involves the pion distribution amplitude (DA) in order to describe the pion bound state. Tuning the DY reaction to the kinematic edge of the phase space, where the antiquark \bar{u} from the pion is far off-shell, i.e., $x_{\bar{u}} \rightarrow 1$, it is sufficient to treat the quark u , originating from the nucleon, as being nearly free and on-mass-shell, so that the bound-state details of the nucleon become irrelevant [4]. In those circumstances the process $MB \rightarrow l^+l^-X$ reduces to $\pi^-u \rightarrow \mu^+\mu^-X$ and the corresponding amplitude becomes calculable within perturbative QCD. The binding effects of the pion state are taken into account by means of the pion DA (which is the pion wave function integrated over transverse momenta), making this type of process suitable to test the details of proposed nonperturbative models for the pion DA.

Moreover, the angular distribution of the produced lepton pair (actually the μ^+), relative to the pion direction, depends in a sensitive way on the pion DA. Hence, measuring the angular distribution parameters λ, μ, ν (for an unpolarized target) and $\bar{\mu}, \bar{\nu}$ (for longitudinally polarized protons), one can extract useful information on the shape of the pion DA [5, 6]. This is particularly important with regard to a proposed experiment by the COMPASS collaboration to collect high-precision data from the scattering of a pion beam off a polarized target [7].

In the present work we will consider (i) the inclusive production of dimuons from the hard scattering of pions on an unpolarized nuclear target and (ii) an analogous process with longitudinally polarized protons. The appearance of a single transverse-spin asymmetry in the latter case is related to an imaginary part, which, may even dominate the dimuon angular distribution [6]. Because this contribution is very sensitive to the pion DA, the single-spin asymmetry can be used in conjunction with the experimental data in order to select the most preferable pion DA. Our attention is focused in both cases on the role played by the pion bound state in terms of the pion DA.

The paper is organized as follows. In the next section, we present the theoretical background of the DY model in πN collisions, taking into account the valence-quark bound state of the pion, which we model with the aid of nonlocal QCD sum rules [8] in comparison with the Chernyak–Zhitnitsky [9] model and the asymptotic pion DA [10, 11, 12]. Section III contains the presentation of our results for the angular distribution parameters λ, μ, ν , and comparison with the data from the E615 experiment at Fermilab [3]. In this section, we also make predictions for the angular parameters $\bar{\mu}$ and $\bar{\nu}$, using the aforementioned pion DAs. Particular attention is devoted to the endpoint behavior of different pion DAs by considering an azimuthal moment of the pion DA, discussed before in [6]. Finally, our conclusions are provided in Sec. IV.

II. DRELL-YAN PROCESS OF DIMUON PRODUCTION

This section describes the theoretical method used to calculate the angular distribution of the μ^+ in the DY process in a πN collision in terms of the parameters λ, μ, ν (unpolarized target) and $\bar{\mu}, \bar{\nu}$ (longitudinally polarized protons).

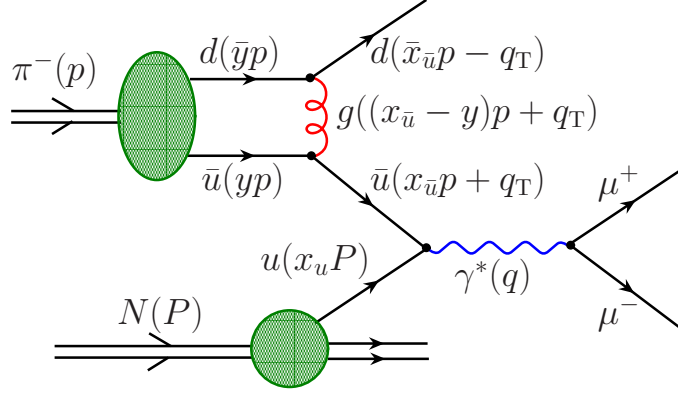


FIG. 1: Graphical representation of the Drell-Yan process $\pi^- N \rightarrow \mu^+ \mu^- X$. Symbols $p = p_\pi$, $P = p_N$ and $q = -x_u P + x_{\bar{u}} p + q_T$, where $x_{\bar{u}} = x_\pi$, and $x_u = x_N$ (see for details Sec. II A), mean four-momenta. Here, and below, solid lines denote leptons and also the quarks emerging from the πN collision, double lines indicate bound states (with their corresponding wave functions being illustrated by shaded blobs), whereas the (red) curly line stands for the exchanged hard gluon and the (blue) weavy line represents the highly virtual photon.

The DY process is the dominant mechanism to produce lepton pairs with a large invariant mass Q^2 in hadronic collisions, like $\pi^\pm N$ scattering. In the context of this model a massive lepton (muon) pair is created through the electromagnetic annihilation of an antiquark from the beam pion and a quark from the nucleon target, as depicted in Fig. 1. Moreover, in the kinematic region of large $x_\pi = x_{\bar{u}} \rightarrow 1$ (or $x_L \rightarrow 1$, see next section), the antiquark in the pion is subject to bound-state effects encoded in the valence-quark pion DA, while the quark from the nucleon is nearly on shell. Then, the pion bound state can be resolved via hard-gluon exchange between the annihilating antiquark and the spectator in convolution with the pion DA [5], displayed diagrammatically in Fig. 2. This provides a means to test the validity of proposed models for the pion DA, derived from nonperturbative QCD calculations, because the angular distribution of the produced muon pair depends in a sensitive way on the shape of the pion DA. Contributions from higher-order hard-gluon exchange are suppressed by powers of α_s and will be ignored; those due to evolution will be taken into account in leading order (LO). Alternatively, ignoring chromodynamic binding effects, one may extract in the context of the DY model, the structure functions of the pion and the nucleon [3, 4] or focus on quark density functions [4, 13]. These issues are outside the scope of the present investigation.

To continue with our quantitative analysis, we first present some explanations on the kinematics of the DY process together with the definitions of the dynamical parameters which describe the angular distribution in the hadronic differential cross section.

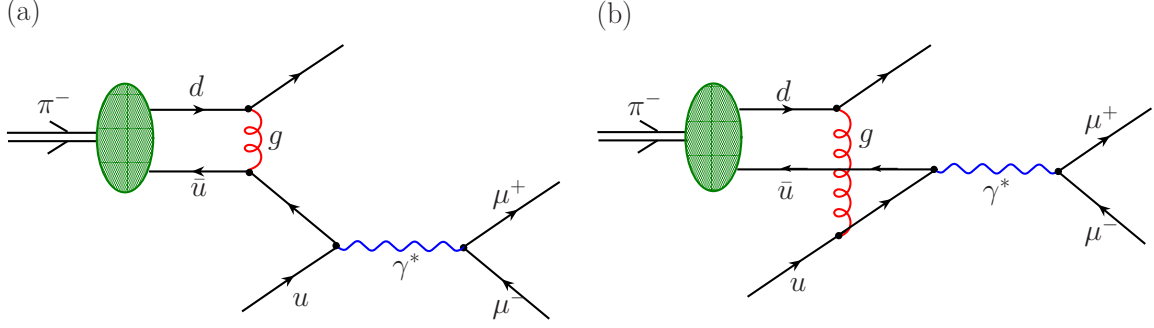


FIG. 2: Leading (perturbative) contributions to the QCD-amplitude describing the Drell-Yan process $\pi^- N \rightarrow \mu^+ \mu^- X$ at large Q^2 and x_L , the latter defined in Eq. (2.9). The designations are the same as in Fig. 1.

A. Kinematics and variables of the DY process

For the convenience of the reader, the relevant kinematic parameters and dynamical variables for the DY process $MB \rightarrow l^+ l^- X$ (with M, B denoting a meson and a baryon, respectively) are compiled below in conceptual groups and in conjunction with Fig. 1:

Momenta

- $p_\pi \equiv p$: Pion momentum.
- $p_N \equiv P$: Nucleon momentum.
- $p_{\bar{u}}$: Momentum of the annihilating antiquark \bar{u} emerging from the pion, $p_{\bar{u}} = x_{\bar{u}} p$. As $x_{\bar{u}} \rightarrow 1$ (i.e., \bar{u} far off-shell), $p_{\bar{u}}^2$ becomes large and far spacelike.
- $x_{\bar{u}}$: Longitudinal momentum fraction (light-cone variable) of the annihilating \bar{u} from the meson. In the kinematical regime, we are considering, $x_{\bar{u}} = x_\pi$.
- $\langle \mathbf{k}_T^2 \rangle$: Average of the square of the transverse momentum of the annihilating \bar{u} from the meson ($\mathbf{k}_T^2 \ll Q^2$).
- p_u : Momentum of the annihilating quark u emerging from the nucleon, $p_u = x_u P$. Because $x_{\bar{u}} \rightarrow 1$, it is sufficient to consider the u -quark to be nearly free and on-shell: $x_u = x_N$ (quark masses and transverse momenta neglected).
- $Q \equiv m_{\mu\mu}$: Invariant mass of the massive lepton (muon) pair, or, equivalently, momentum of the virtual photon created by the annihilated quarks ($Q^2 = q^2$). In this analysis we consider values in the range $Q^2 = (4 - 81) \text{ GeV}^2$.
- s : Squared invariant mass of the initial hadrons, i.e., $s = (p + P)^2$. In our numerical analysis we use $s = 100 - 400 \text{ GeV}^2$, which covers the 252 GeV π^- beam of the E615 Collaboration at Fermilab [3].

Masses

- m_π : Pion mass. Because $s \gg m_\pi^2$, we set $m_\pi = 0$.

- m : Bare quark mass. Because $s \gg m^2$, we set $m = 0$;
- m_N : Nucleon mass.

Kinematic Variables

- $\tau \equiv Q^2/s$: Scaling parameter.
- $\rho \equiv Q_T/Q$: This scaling parameter is a measure for the squared transverse momentum $Q_T^2 \equiv -q_T^2$ of the virtual photon in the hadronic center-of-mass frame (c.m.f.). Inspection of Fig. 1 reveals that q_T appears only in combination with $x_{\bar{u}}p$, namely, $q_T + x_{\bar{u}}p$. Then, in order to separate both terms unambiguously, one has to demand that q_T should not contain any part of the pion momentum p , cf. Eq. (2.6).
- $x_L = 2Q_L/\sqrt{s} < 1$: Longitudinal momentum fraction (Feynman x) of the lepton pair (associated with the virtual photon) in the hadron c.m.f. ($Q_L^2 = q_L^2$). Q_L and Q_T are the photon-momentum components parallel and perpendicular, respectively, to the incident pion momentum in the hadron c.m.f.
- $x_F = x_\pi - x_N$ and $x_\pi x_N = \tau$. Neglecting the quark transverse momentum and mass (as s becomes very large), the quantities x_π and x_N can be identified with $x_{\bar{u}}$ and x_u , respectively. Combining the two equations above, one finds [3] $x_{\pi,N} = [\pm x_F + (x_F^2 + 4\tau)^{1/2}] / 2$.

Angular distribution parameters

- θ : Polar angle measuring the μ^+ direction with respect to the t -channel (or Gottfried–Jackson system of axes), i.e., $\cos \theta = \hat{p}_\mu \cdot \hat{p}_\pi$. The definitions of other choices of axes (frames) can be found, e.g., in [3].
- ϕ : Azimuthal angle between the massive lepton-pair plane and the plane of the incident hadrons in the lepton rest frame.
- λ, μ, ν : Angle-independent coefficients, depending on Q^2 and x_L . These three parameters control the dilepton angular distribution and are sensitive to the shape of the pion DA.
- $\bar{\mu}, \bar{\nu}$: Angle-independent coefficients, depending on Q^2 and x_L , induced by the imaginary part to the DY amplitude in the polarized case. They are sensitive to the shape of the pion DA.

In our analysis we consider values of s much larger than the nucleon mass, $s \geq 100 m_N^2$, so that this be neglected, though we derive the exact result with $m_N^2 \neq 0$ and proceed then with the approximate expression with $m_N = 0$, where it is applicable. The momenta p and P are on the light-cone and, hence, we have

$$p^2 = 0, \quad P^2 = m_N^2 \approx 0, \quad 2(p \cdot P) = s - m_N^2 \equiv \tilde{s} \approx s. \quad (2.1)$$

For the cross-section calculation, one can appeal to the optical theorem and set the upper right line in Fig. 1, denoting the d -quark, on mass shell. Then,

$$2(p \cdot q_T) = \frac{q_T^2}{1 - x_{\bar{u}}} = \frac{-\rho^2 Q^2}{1 - x_{\bar{u}}} \quad (2.2)$$

and, due to $q = (x_u + x_{\bar{u}})p + q_T$, one obtains

$$\begin{aligned} Q^2 &= (s - m_N^2) x_u x_{\bar{u}} \left[1 + \frac{x_u m_N^2}{x_{\bar{u}} (s - m_N^2)} \right] - \frac{\rho^2 Q^2}{1 - x_{\bar{u}}} \left(1 + \frac{2 x_u m_N^2}{s} \right) \\ &\approx s x_u x_{\bar{u}} \left(1 + \frac{x_u m_N^2}{x_{\bar{u}} s} \right) - \frac{\rho^2 Q^2}{1 - x_{\bar{u}}}, \end{aligned} \quad (2.3)$$

or

$$\begin{aligned} x_u x_{\bar{u}} &= \left[1 + \frac{\rho^2}{1 - x_{\bar{u}}} \left(1 + \frac{2 x_u m_N^2}{s} \right) \right] \frac{Q^2}{\tilde{s} + m_N^2 (x_u/x_{\bar{u}})} \\ &\approx \left(1 + \frac{\rho^2}{1 - x_{\bar{u}}} \right) \tau \left(1 - \frac{x_u m_N^2}{x_{\bar{u}} s} \right), \end{aligned} \quad (2.4)$$

which fixes the value of x_u as a function of $x_{\bar{u}}$, ρ and τ . We also see that a non-zero nucleon mass is important only at very small $x_{\bar{u}} \simeq m_N^2/s$. At this value of $x_{\bar{u}}$ the value of x_u is close to 1, so that, neglecting m_N , one finds $1/[1 + (m_N^2/Q^2)/(1 + \rho^2)]$. Hence, the difference can be sizable and, especially at $Q^2 \sim 2m_N^2$ and $\rho \sim 1$, it can reach as much as 20%.

In the following considerations (and, in particular, in the analysis of the polarized DY process), we will use the longitudinal-momentum fraction of the photon, x_L . To this end, recall that in the hadron c.m.f. one has

$$p = \frac{\sqrt{s}}{2}(1, 0, 0, +1), \quad P = \frac{\sqrt{s}}{2}(1, 0, 0, -1), \quad q_{\perp} = (0, q_{\perp 1}, q_{\perp 2}, 0) \quad (2.5)$$

and, using Eq. (2.2), one finds

$$q_T = q_{\perp} - a_T P, \quad a_T \equiv \frac{\rho^2 \tau}{1 - x_{\bar{u}}}, \quad (2.6)$$

$$q = q_{\perp} + q_L, \quad q_L = x_{\bar{u}} p + (x_u - a_T) P = \frac{\sqrt{s}}{2}(x_0, 0, 0, x_L), \quad (2.7)$$

with x_L being defined by

$$x_0 = x_{\bar{u}} + x_u - a_T, \quad x_L = x_{\bar{u}} - x_u + a_T. \quad (2.8)$$

It is convenient to recast x_L in terms of $x_{\bar{u}}$, ρ , and τ to read

$$x_L = x_{\bar{u}} - \frac{1 + \rho^2}{x_{\bar{u}}} \tau. \quad (2.9)$$

The inverse relation

$$x_{\bar{u}} = \frac{x_L + \sqrt{x_L^2 + 4(1 + \rho^2)\tau}}{2} \quad (2.10)$$

defines $x_{\bar{u}}$ as a function of x_L , ρ , and τ .

B. Drell–Yan πN process with a pion bound state

There have been attempts [5] and, in particular [6], to test the compatibility of different pion DAs with the DY angular distribution measured in the scattering of pions off protons. The first work suggested that the CZ pion DA (and some variant of it) fits the unpolarized data [3] better than the asymptotic DA, or narrower convex versions [13]. The second work focused on the possibility of longitudinally polarized protons as a target and discussed additional angular parameters that vanish for an unpolarized target. It was argued that future polarized experimental data on these processes may be able to distinguish among various pion DAs because of the high sensitivity of these parameters to the particular shape of the pion DA. Though there is still no such data available, meanwhile important knowledge has been collected that is rather unfavorable for the endpoint-dominated type of two-humped pion DAs, like the CZ one. For instance, new high-precision lattice simulations [14, 15, 16] give a new level of detail for the second Gegenbauer coefficient a_2 , yielding values around 0.2 to 0.24 at a momentum scale of 2 GeV, well within the range suggested by the nonlocal QCD sum-rule estimates [8]—hereafter referred to as BMS—and supported by the analysis in [17, 18, 19] of the CLEO data [20] on the $\pi - \gamma$ transition form factor using light-cone QCD sum rules. This a_2 value is about two times smaller than its counterpart of the CZ pion DA and cast serious doubts about the consistency of this model with experiment. Moreover, the aforementioned BMS CLEO-data analysis has confirmed the earlier Schmedding and Yakovlev [21] findings which excluded the CZ pion DA at least at the 2σ level. On the other hand, the asymptotic pion DA seems to be also excluded, given that its Gegenbauer coefficient a_2 is identically zero and the CLEO-data analysis relegates this DA outside the 2σ error ellipse (for the most recent rigorous analysis, see [19]), while being also incompatible with the lattice results [14, 15, 16]. Further theoretical arguments and details can be found in [22]. See also [23] for a recent development of the nonlocal QCD sum-rule approach and the extraction of the pion DA.

Therefore, it would seem reasonable and timely to upgrade the calculation of the DY angular parameters of the $\pi^- N$ hard-scattering process by taking into account the recent developments quoted above. To continue, we first recall the definition of the pion DA, $\varphi_\pi(y, \mu_0^2)$, which specifies the fractional longitudinal momentum y of the valence-quark constituents in the pion at the normalization scale μ_0^2 . At the (leading) twist-two level it is defined by the following matrix element

$$\langle 0 | \bar{d}(z) \gamma^\mu \gamma_5 \mathcal{C}(z, 0) u(0) | \pi(P) \rangle \Big|_{z^2=0} = iP^\mu f_\pi \int_0^1 dy e^{iy(zP)} \varphi_\pi(y, \mu_0^2) , \quad (2.11)$$

$$\int_0^1 \varphi_\pi(y, \mu_0^2) dy = 1 , \quad (2.12)$$

where $f_\pi = 130.7 \pm 0.4$ MeV [24] is the pion decay constant defined by

$$\langle 0 | \bar{d}(0) \gamma_\mu \gamma_5 u(0) | \pi^+(P) \rangle = ip_\mu f_\pi . \quad (2.13)$$

Above, a straight path-ordered Fock–Schwinger connector [25] (Wilson line) $\mathcal{C}(0, z) = \mathcal{P} \exp[-ig_s \int_0^z t^a A_\mu^a(y) dy^\mu]$ has been inserted to preserve gauge invariance of the operator product. In the following, we use the light-cone gauge which reduces the contribution of the Wilson line to unity. The normalization scale, μ_0^2 , of the pion DA is related to the ultraviolet (UV) regularization of the quark-field operators on the light cone in (2.12), whose product becomes singular for $z^2 = 0$.

The pion DA cannot be derived from first principles, but has to be inferred from non-perturbative QCD models (or from experiment). This notwithstanding, its evolution is governed by perturbative QCD [10, 11, 12] and can be expressed in the form

$$\varphi_\pi(y, \mu^2) = U(y, s; \mu^2, \mu_0^2) \otimes_s \varphi_\pi(s, \mu_0^2), \quad \otimes_s \equiv \int_0^1 ds, \quad (2.14)$$

where $\varphi_\pi(s, \mu_0^2)$ is a nonperturbative input determined at some low-energy normalization point $\mu_0^2 \sim 1 \text{ GeV}^2$, where the local operators in Eq. (2.11) are renormalized, while $U(y, s; \mu^2, \mu_0^2)$ is the evolution operator from that scale to the observation scale μ , calculable in QCD perturbation theory. In the asymptotic limit, the shape of the pion DA is completely fixed by pQCD to be $\varphi_\pi^{\text{asy}}(y) = 6y(1-y)$ [10, 11, 12], with the nonperturbative information being solely contained in the pion-decay constant f_π .

In the leading-twist approximation of the pion DA, in which we are working, $\varphi_\pi(y, \mu_0^2)$ can be expressed in terms of the Gegenbauer polynomials, which form an orthonormal set of eigenfunctions. Then,

$$\varphi_\pi(y, \mu_0^2) = 6y(1-y) \left[1 + a_2(\mu_0^2) C_2^{3/2}(2y-1) + a_4(\mu_0^2) C_4^{3/2}(2y-1) + \dots \right], \quad (2.15)$$

with all nonperturbative information being encapsulated in the expansion coefficients a_n . Depending on the nonperturbative approach applied, these coefficients can be calculated via QCD sum rules [9], QCD sum rules with nonlocal condensates [8], or lattice simulations [14, 15, 16, 26]. More details can be found in the original papers already cited, while we here restrict ourselves to the obtained results, which we quote in Table I. The shapes of these DAs are displayed in the left panel of Fig. 3, whereas the evolution effect is illustrated in the right panel of this figure in terms of the BMS pion DA. Note that the underlying quark virtuality employed, is $\lambda_q^2 = 0.4 \text{ GeV}^2$ [17] corresponding to a correlation length of the scalar quark nonlocal condensate of about 0.31 fm. As one anticipates from this figure, the key characteristic of the BMS-type pion DAs is that the endpoint region $x \rightarrow 0, 1$ is strongly suppressed—not only relative to the CZ pion DA, but even with respect to the asymptotic one (for mathematical details, see [22]). In contrast, the double-humped shape—reminiscent of the CZ pion DA—turns out to be of minor importance [27].

TABLE I: Pion DA models used in the analysis.

π -DAs $_{\mu^2=1 \text{ GeV}^2}$	asymptotic	BMS [8]	BMS “bunch” [8, 18]	CZ [9]
a_2	0	0.20	[0.13, 0.25]	0.56
a_4	0	−0.14	[−0.04, −0.22]	0
higher	0	negligible	negligible	0

Let us now make some remarks on the evolution of the pion DA in LO of perturbative QCD. Taking into account only the first two Gegenbauer coefficients, one obtains

$$\varphi_\pi^{\text{LO}}(y, \mu_F^2) = 6y(1-y) \left[1 + a_2^{\text{LO}}(\mu_F^2) C_2^{3/2}(2y-1) + a_4^{\text{LO}}(\mu_F^2) C_4^{3/2}(2y-1) \right], \quad (2.16)$$

where $a_2^{\text{LO}}(\mu_F^2)$ and $a_4^{\text{LO}}(\mu_F^2)$ are given by

$$a_n^{\text{LO}}(\mu_F^2) = a_n(\mu_0^2) \left[\frac{\alpha_s(\mu_F^2)}{\alpha_s(\mu_0^2)} \right]^{\gamma_n^{(0)}/(2b_0)}. \quad (2.17)$$

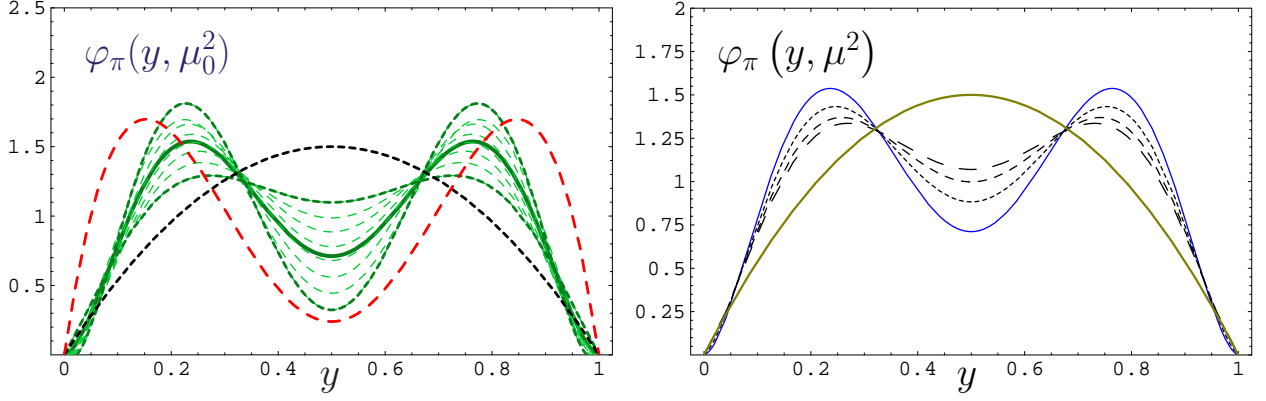


FIG. 3: The left panel shows the “bunch” of pion DAs (green broken lines), derived from nonlocal QCD sum rules (for a summarized exposition, see, e.g., [22]), in comparison with two extreme alternatives: the asymptotic DA [10, 11, 12]—dotted line—and the CZ model [9]—red long-dashed line—at the momentum scale $\mu^2 \approx 1 \text{ GeV}^2$. The green solid line inside the “bunch” represents the BMS model [8]. The right panel illustrates the effect of one-loop evolution on the pion DA, exemplified by the BMS model, in comparison with the asymptotic solution (continuous convex line). The double-humped solid line represents $\varphi_{\text{BMS}}^{\text{LO}}(x)$ at 1 GeV^2 , while the broken lines mark $\varphi_{\text{BMS}}^{\text{LO}}(x)$ at 4, 20, and 100 GeV^2 (with the larger scale corresponding to the larger value of the DA at the middle point).

The expressions for the anomalous dimensions $\gamma_n^{(0)}$ and the beta-function coefficient b_0 are listed, for example, in [17]. One sees from the right panel of Fig. 3 that the effect of the inclusion of the LO diagonal part of the evolution kernel is indeed important. This figure shows how the BMS pion DA $\varphi_{\text{BMS}}^{\text{LO}}(x)$ evolves from the normalization scale of 1 GeV^2 (double-humped solid line) to higher momentum values at 4, 20, and 100 GeV^2 (broken lines), with the larger scales corresponding also to larger values of the DA at the middle point. The asymptotic profile (continuous solid line) is displayed for comparison.

C. DY reaction with an unpolarized target

The angular distribution of the μ^+ in the pair rest frame can be written in terms of the kinematic variables λ, μ, ν as follows

$$\frac{d^5\sigma(\pi^- + N \rightarrow \mu^+ + \mu^- + X)}{dQ^2 dQ_T^2 dx_L d\cos\theta d\phi} \propto N(\tilde{x}, \rho) \left(1 + \lambda \cos^2\theta + \mu \sin 2\theta \cos\phi + \frac{\nu}{2} \sin^2\theta \cos 2\phi \right), \quad (2.18)$$

where [5]

$$\lambda(\tilde{x}, \rho) = \frac{2}{N} \left\{ (1 - \tilde{x})^2 [(\text{Im } I(\tilde{x}))^2 + (F + \text{Re } I(\tilde{x}))^2] - (4 - \rho^2) \rho^2 \tilde{x}^2 F^2 \right\}, \quad (2.19)$$

$$\mu(\tilde{x}, \rho) = -\frac{4}{N} \rho \tilde{x} F \left\{ (1 - \tilde{x}) [F + \text{Re } I(\tilde{x})] + \rho^2 \tilde{x} F \right\}, \quad (2.20)$$

$$\nu(\tilde{x}, \rho) = -\frac{8}{N} \rho^2 \tilde{x} (1 - \tilde{x}) F [F + \text{Re } I(\tilde{x})], \quad (2.21)$$

$$N(\tilde{x}, \rho) = 2 \left\{ (1 - \tilde{x})^2 [(\text{Im } I(\tilde{x}))^2 + (F + \text{Re } I(\tilde{x}))^2] + (4 + \rho^2) \rho^2 \tilde{x}^2 F^2 \right\} \quad (2.22)$$

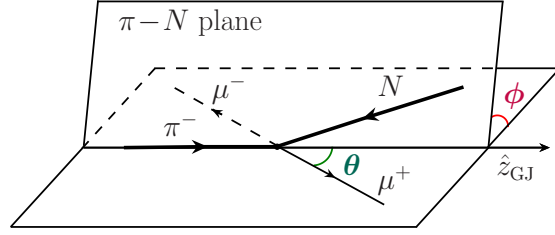


FIG. 4: Angular definitions of the Drell–Yan process in the center of mass frame of the produced massive lepton pair. The axis \hat{z}_{GJ} denotes the pion direction in the Gottfried–Jackson (GJ) frame.

with

$$\tilde{x}(x_L, \rho) \equiv \frac{x_L + \sqrt{x_L^2 + 4(1 + \rho^2)\tau}}{2(1 + \rho^2)}. \quad (2.23)$$

Also displayed is the normalization factor of the cross section, N . The abbreviations

$$F = \int_0^1 dy \frac{\varphi(y, \tilde{Q}^2)}{y} \quad (2.24)$$

$$I(\tilde{x}) = \int_0^1 dy \frac{\varphi(y, \tilde{Q}^2)}{y(y + \tilde{x} - 1 + i\varepsilon)} \quad (2.25)$$

are functionals of the pion DA and, therefore, depend on the evolution momentum scale $\tilde{Q}^2 \sim Q^2$. Note that the inverse moment (2.24) of the pion DA plays a crucial role in the description of several form factors of the pion in perturbative QCD [27]. We will have more to say about the choice of the evolution scale in the next subsection. Note also that the denominators in Eqs. (2.24) and (2.25) originate from the gluon and quark propagators in the subprocesses shown in Fig. 2, respectively. Before presenting results for these angular coefficients, let us first discuss what changes are induced when the nuclear target is polarized.

D. DY reaction with longitudinally polarized protons

In the polarized DY process the angular distribution of the μ^+ contains two additional parameters $\bar{\mu}$ and $\bar{\nu}$, entering additively Eq. (2.18) with the same angular structure as μ and ν , respectively, being, however, proportional to the target longitudinal polarization s_ℓ :

$$\bar{\mu}(\tilde{x}, \rho) = \frac{-2\pi s_\ell \rho \tilde{x} F \varphi(\tilde{x}, \tilde{Q}^2)}{(1 - \tilde{x})^2 [(F + \mathbf{Re} I(\tilde{x}))^2 + \pi^2 \varphi(\tilde{x})^2] + (4 + \rho^2) \rho^2 \tilde{x}^2 F^2} \bar{\mu}_{\text{nucl}}, \quad (2.26)$$

$$\bar{\mu}_{\text{nucl}} \equiv \frac{\frac{4}{9} \Delta q_u^v(x_p; \mu^2) + \frac{4}{9} \Delta q_u^s(x_p; \mu^2) + \frac{1}{9} \Delta q_d^s(x_p; \mu^2)}{\frac{4}{9} q_u^v(x_p; \mu^2) + \frac{4}{9} q_u^s(x_p; \mu^2) + \frac{1}{9} q_d^s(x_p; \mu^2)}, \quad (2.27)$$

$$\bar{\nu}(\tilde{x}, \rho) = 2\rho \bar{\mu}(\tilde{x}, \rho). \quad (2.28)$$

where $x_p = \tau/\tilde{x}$, μ^2 is the evolution scale for the nucleon parton distributions. Note that all momenta refer to the hadronic c.m.f. The polarized parton distributions used in our

analysis are taken from [28], whereas for the unpolarized structure functions we use the parameterization of Ref. [29]. To evolve these distributions from their normalization scale $\mu_0^2 = 4 \text{ GeV}^2$ to the scale $\mu^2 = Q^2 = 16 \text{ GeV}^2$, we employed the Fortran codes supplied by the authors of these papers on the Durham web site.¹

Lacking radiative corrections to the process under study, we cannot fix the evolution scale unambiguously. In an effort to get a measure for the entailed uncertainty, we have analyzed the dependence of our results on the choice of the evolution scale by varying μ^2 in the range $\mu^2 = Q^2/2$ and $\mu^2 = 2Q^2$. We found that, depending on the model pion DA used, the variance of the calculated $\bar{\mu}$ parameter lies between 2% and 17%, with moderate sensitivity to the adopted ρ value. Details are given in Table II for the (large) x_L interval, in which the one-gluon exchange is still a good approximation and only the pion bound-state is of importance. Recall in this context that the only evolution effect in the case of the asymptotic pion DA stems exclusively from the DGLAP evolution of the nucleon parton distributions. On the other hand, in the case of the BMS and the CZ pion DAs, the total evolution effect is the result of the combination of the ERBL evolution of the pion DA and the DGLAP evolution of the nucleon parton distributions (unpolarized and polarized) in μ_{nuc} (cf. Eq. (2.27)).

TABLE II: Change of predictions for $\bar{\mu}(x_L, \rho)$, shown in Fig. 7, due to different settings of the evolution scale.

π -DAs	asymptotic	BMS [8]	CZ [9]
$\rho = 0.06$ and $0.5 \leq x_L \leq 0.84$	2.0 – 2.5%	12 – 2.5 %	17 – 2.5 %
$\rho = 0.30$ and $0.5 \leq x_L \leq 0.83$	2.0 – 2.5%	9 – 0 %	13 – 0 %
$\rho = 0.50$ and $0.5 \leq x_L \leq 0.81$	1.5 – 2.0%	8 – 0 %	13 – 8 %

It was noted in [6] that the angular moment of the pion DA, defined by

$$\mathcal{M}_{\text{ang}} = \int \sin 2\theta \sin \phi d\sigma(s_\ell = 1) = -2\pi\rho\tilde{x}F\varphi(\tilde{x}, \tilde{Q}^2)\bar{\mu}_{\text{nuc}}, \quad (2.29)$$

is particularly sensitive to the \tilde{x} (or x_L) endpoint region and can be used in comparison with experimental data in order to distinguish pion DAs which behave differently exactly in this region. We have, therefore, included predictions also for this quantity (see next section, Fig. 8). In similar context, it is important to consider the (experimental) single-spin azimuthal asymmetry (SSA)

$$\mathcal{A} \equiv \frac{d\sigma(s_\ell = +1) - d\sigma(s_\ell = -1)}{d\sigma(s_\ell = +1) + d\sigma(s_\ell = -1)} \quad (2.30)$$

after averaging the cross sections over the polar angle $\theta \in [0, \pi]$:

$$\mathcal{A}(\phi, x_L, \rho) = \frac{\rho\bar{\mu}(s_\ell = +1)\sin 2\phi}{2 + \lambda + \frac{1}{2}\nu\cos 2\phi}. \quad (2.31)$$

In Eq. (2.30), $\sigma(s_\ell = +1)$ and $\sigma(s_\ell = -1)$ denote opposite helicity states of the longitudinally polarized target. Notice that in order that the longitudinally polarized nucleon parton

¹ <http://durpdg.dur.ac.uk/hepdata/grv.html> — for GRV95 and
<http://durpdg.dur.ac.uk/pdflib/gehrmann/pdf/welcome.html> — for GS96.

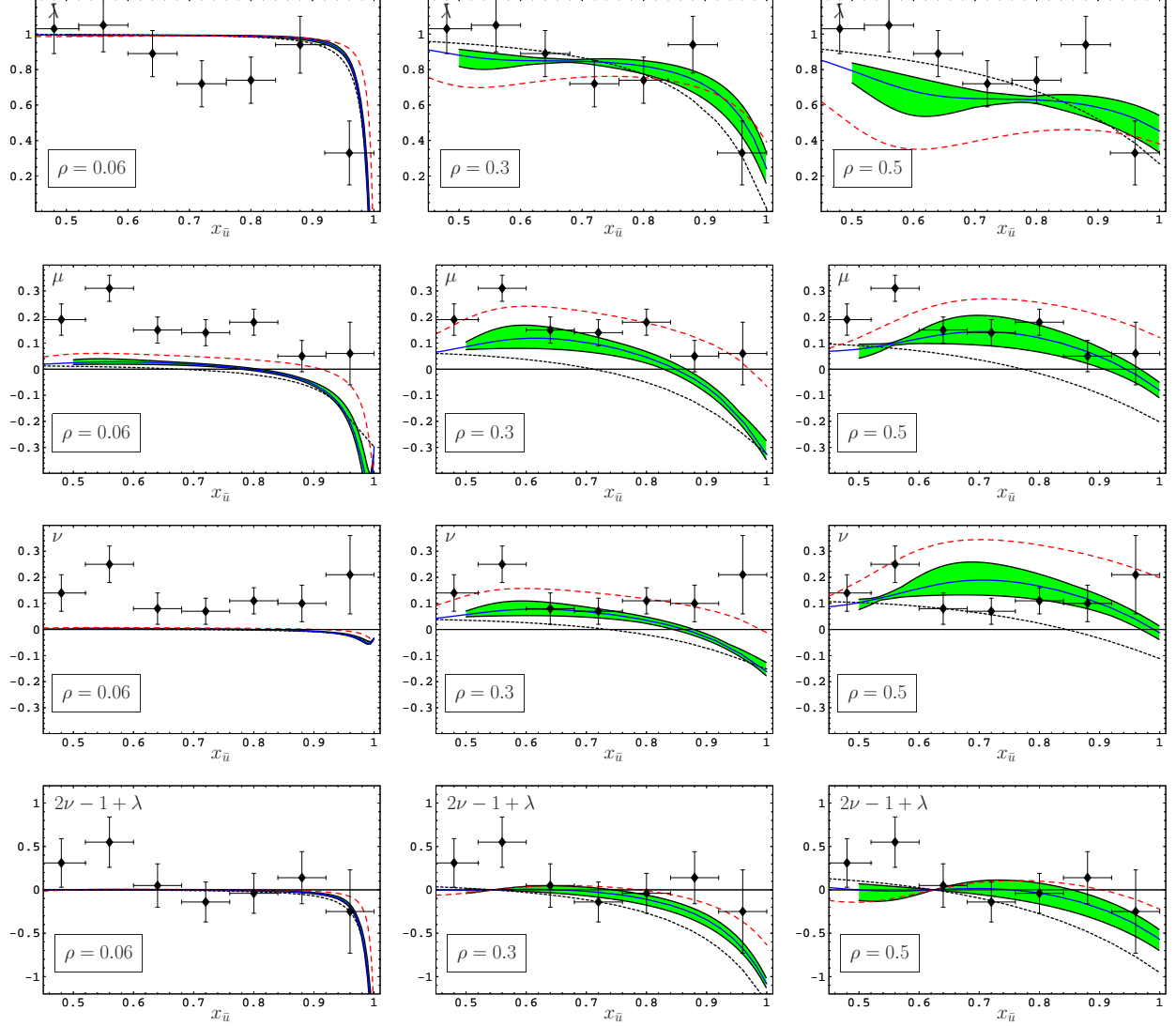


FIG. 5: Results for the angular distribution parameters λ , μ , and ν as functions of $x_{\bar{u}} \equiv x_{\pi}$ for different values of $\rho \equiv Q_T/Q$. Predictions for the Lam–Tung [30] combination, $2\nu - (1 - \lambda)$, are also displayed. The green strip contains the results for the pion DAs calculated with nonlocal QCD sum rules [8, 17, 18]. The (blue) solid line corresponds to one of these endpoint-suppressed DAs, termed BMS, while the dotted (black) solid line shows the result for the asymptotic DA, and the (red) dashed line is the prediction for the endpoint-dominated Chernyak–Zhitnitsky DA [9]. One-loop evolution of the pion DAs to each measured Q^2 value is included. The data were taken from [3] and were evaluated as explained in the text.

distributions can transfer its polarization to the azimuthal distribution of the massive lepton pair, one needs an imaginary part and the interference of amplitudes with a phase difference between them. Both ingredients are provided here by the pion DA and the hard-gluon exchange. Ignoring pion bound-state effects in the treatment of the DY process, one would have to include in the hard cross sections perturbative QCD radiative corrections proportional to α_s in order to create a SSA.

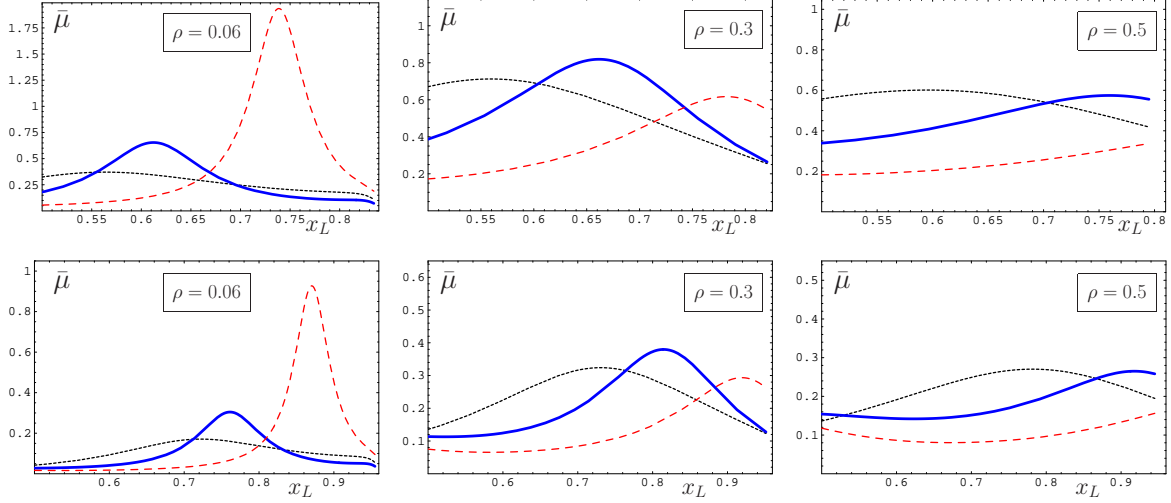


FIG. 6: Angular parameter $\bar{\mu}(x_L, \rho)$ as a function of x_L for three different pion DAs, evaluated at three different values of the scaling parameter ρ using one-loop evolution. Results are shown for the asymptotic pion DA [10, 11, 12] (black dotted line), the BMS model [8] (blue solid line) and the CZ one [9] (red dashed line). The upper row corresponds to a center-of-mass energy $s = 100 \text{ GeV}^2$, whereas the lower one has $s = 400 \text{ GeV}^2$.

III. COMPARISON WITH EXPERIMENTAL DATA

In this section we present our results for the angular distribution parameters λ, μ, ν (versus $x_\pi \rightarrow x_{\bar{u}}$) for the unpolarized DY process and compare them with the available experimental data. We also include predictions for the parameter $\bar{\mu}$ (versus x_L), which is nonzero only in the polarized DY process, and the SSA \mathcal{A} .

All results were obtained using different models for the pion DA, already mentioned, and they are shown at different values of Q_T , i.e., at different values of the scaling parameter ρ .

To be specific, we compare in Fig. 5 our theoretical predictions for λ, μ, ν with experimental data from E615 [3] in that x_π region reported by this collaboration using a 252 GeV π^- beam interacting in an unpolarized tungsten target.

We used for convenience the Gottfried–Jackson frame and included in our analysis the data sample listed in their Table VIII. Because the range of the probed transverse photon momentum, Q_T , is in our opinion too large for averaging, we followed another strategy than the authors in Ref. [5]. Notably, we adopted some value of the scaling parameter $\rho = Q_T/Q$ and required the momenta Q_T and Q to be within the reported window of the measurement in [3]. We evaluated this way the angular parameters shown in the figures, obtained with different pion DAs, including one-loop ERBL evolution with $Q^2 = m_{\mu\mu}^2$, and for three different values of $\rho = 0.06, 0.3, 0.5$, whereas $s = 500 \text{ GeV}^2$ in accordance with [3]. Strictly speaking, the results at too low values of $\rho \lesssim 0.06$ are, actually, not compatible with factorization because then Q_T becomes of the order of Λ_{QCD} . They are shown here merely for illustration purposes.

One important observation from Fig. 5 is that the parameter μ increases proportionally with ρ , as it is qualitatively expected from Eq. (2.20) (though there is an additional term proportional to ρ^3 , absent in the parton DY model). This increase turns out to be small for the asymptotic DA [10, 11, 12], whereas it becomes rather too strong for the CZ model [9], while for the BMS strip [8] this enhancement with ρ is moderate and provides best agree-

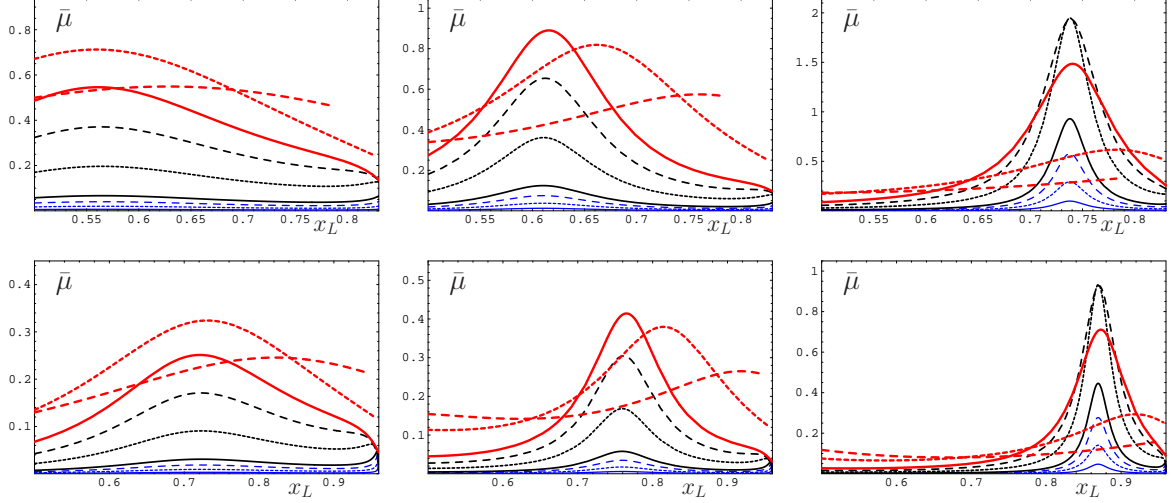


FIG. 7: Evolution effect on the angular parameter $\bar{\mu}(x_L, \rho)$ vs. x_L in several steps of the scaling parameter ρ . Results are shown for the asymptotic pion DA [10, 11, 12] (left panel), the BMS model DA [8] (central panel) and the CZ one [9] (right panel). The following designations are used: The solid lines within each color group correspond to the smallest ρ value. The short-dashed lines denote the results for the intermediate ρ values, whereas the long-dashed lines represent the results with the largest ρ values. The group of the blue lines covers the range $\rho = 0.001, 0.003, 0.006$; the group of black lines gives the results for $\rho = 0.01, 0.03, 0.06$, whereas the red lines are associated with the values $\rho = 0.1, 0.3, 0.5$. The upper row corresponds to a center-of-mass energy $s = 100 \text{ GeV}^2$, whereas the lower one has $s = 400 \text{ GeV}^2$.

ment with the data. A similar behavior is seen also for ν in this figure, which, according

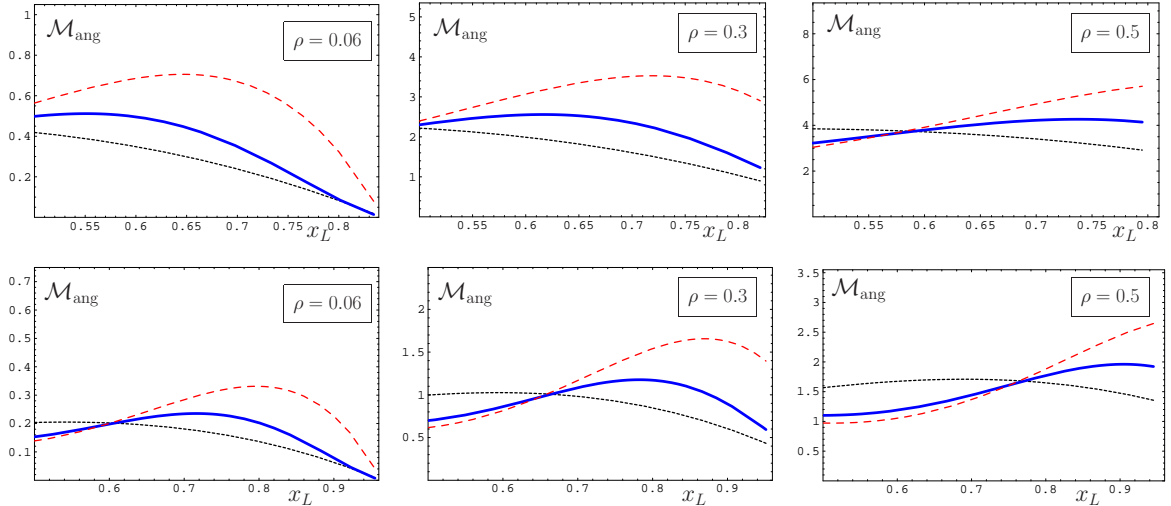


FIG. 8: Angular momentum \mathcal{M}_{ang} as a function of x_L for three different pion DAs, evaluated at three different values of the scaling parameter ρ using one-loop evolution. Results are shown for the asymptotic pion DA [10, 11, 12] (black dotted line), the BMS model [8] (blue solid line) and the CZ one [9] (red dashed line). The upper row corresponds to a center-of-mass energy $s = 100 \text{ GeV}^2$, whereas the lower one has $s = 400 \text{ GeV}^2$.

to Eq. (2.21), should increase proportionally to ρ^2 . Also here the BMS strip compares most favorably with the data relative to the other options. On the other hand, the Lam–Tung combination $2\nu - 1 + \lambda$ [30], which is the analogue of the Callan–Gross relation in deeply inelastic scattering (and also reflects the kinematical nature of the azimuthal asymmetry [31]), is badly violated by the data.

This trend is in agreement with the theoretical predictions above approximately $x_{\bar{u}} \sim 0.6$, though, at very large $x_{\bar{u}}$ close to the kinematic limit, all tested model DAs tend to fall stronger than the data.

Turn now attention to the polarized case. Figure 6 shows the predictions for the angular parameter $\bar{\mu}$ as a function of x_L for three different values of $\rho = 0.06, 0.3, 0.5$ and two center-of-mass-energies $s = 100 \text{ GeV}^2$ (upper row) and $s = 400 \text{ GeV}^2$ in the range expected to be covered in the COMPASS experiment. As before, the results shown were obtained for the asymptotic, BMS, and CZ pion DAs. [Similar results (not shown) hold also for the parameter ν , which is interlinked with μ .]

The result of LO evolution of the pion DA as well as of the nucleon structure functions in the angular parameter $\bar{\mu}$ is the detailed image of curves shown in Fig. 7.

To unravel the behavior of the various pion DAs in the endpoint region, we also examine the angular moment (cf. Eq. (2.29)) and display the results in Fig. 8. As mentioned in the previous section, this quantity was proposed in [6] as a sensitive measure for the angular modulation of the pion DA at large x_L . One sees from this figure that this seems indeed to be the case, especially for not too small ρ values and, once experimental data will become available, it could potentially serve to discriminate among different pion DAs.

To complete the analysis, we include 3D-plots of the parameter $\bar{\mu}$ as a function of x_L and ρ

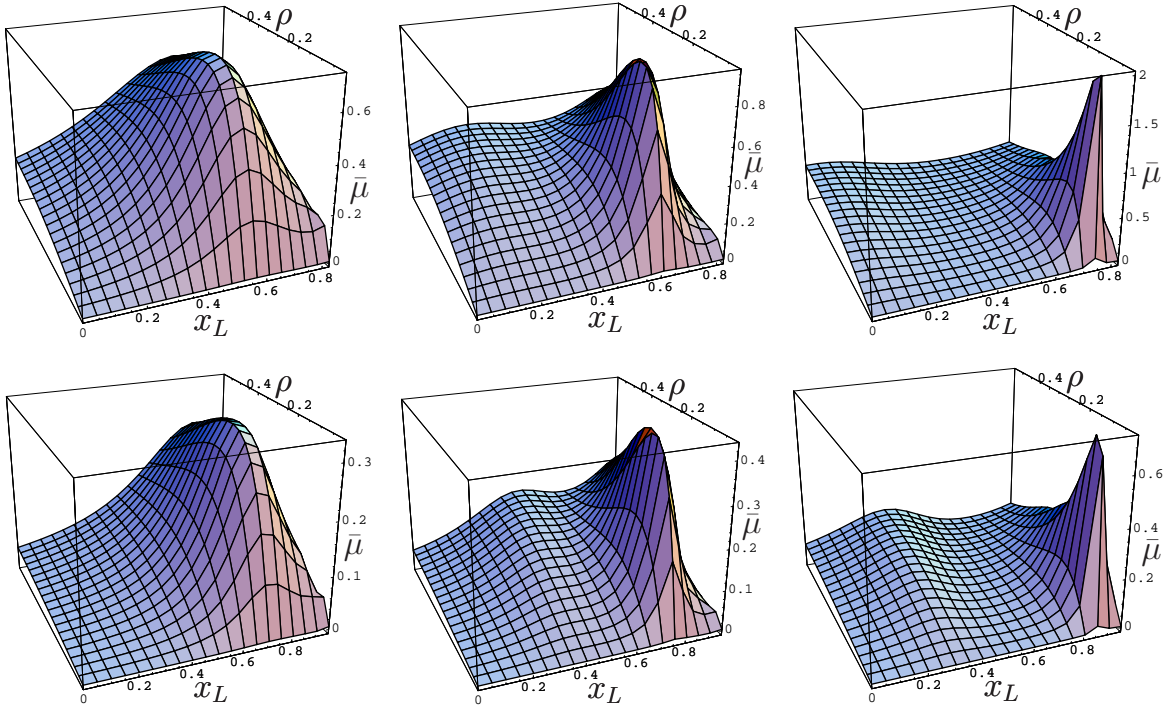


FIG. 9: 3D-plots of the angular parameter $\bar{\mu}(x_L, \rho)$ for three different choices of the pion DA: Asymptotic [10, 11, 12] (left), BMS model [8] (center), and CZ model [9] (right). The upper row corresponds to a center-of-mass energy $s = 100 \text{ GeV}^2$, whereas the lower one has $s = 400 \text{ GeV}^2$.

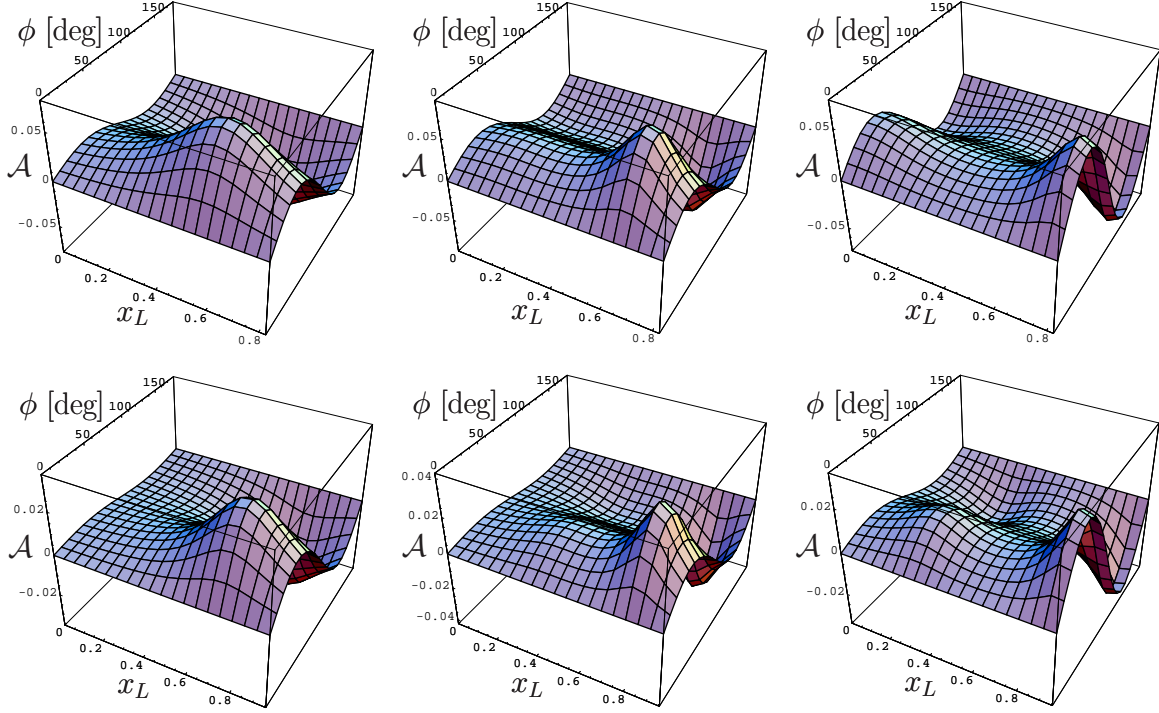


FIG. 10: 3D-plots of the azimuthal asymmetry $\mathcal{A}(\phi, x_L, \rho = 0.3)$. All assignments are as in Fig. 9.

(Fig. 9) and analogously 3D plots of the angular asymmetry $\mathcal{A}(\phi, x_L, \rho)$ versus x_L and ϕ (Fig. 10), the latter for $\rho = 0.3$. Note that both quantities have been evaluated for two different values of the center-of-the-mass energy $s = 100 \text{ GeV}^2$ (upper rows) and $s = 400 \text{ GeV}^2$ (lower rows), as expected for the COMPASS experiment [7].

The observed increase of \mathcal{A} with x_L suggests that the single-spin asymmetry of the muon-pair angular distribution is associated with the valence Fock-state contributions in the pion DA. This behavior is valid for all considered pion DAs and does not significantly depend on the value of the scaling parameters ρ and τ , though its size decreases with increasing s . We have verified that the results do not change significantly for larger ρ values. If future experimental data would confirm such a single-spin asymmetry, this would point to a new mechanism for generating a new nontrivial phase in QCD factorization leading to T-odd spin asymmetries that mimics the effect of a true T violation.

IV. CONCLUSIONS

Our objective in this work was (i) to update previous results on the unpolarized $\pi^- N \rightarrow \mu^+ \mu^- X$ DY process and (ii) to make detailed predictions for the angular distribution parameters for the hard-scattering of pions on longitudinally polarized protons. The single-spin asymmetry, predicted here for various pion distribution amplitudes, may soon become amenable to experimental check at COMPASS. To this end, we have presented an updated analysis of the DY process with the inclusion of the pion's DA, the latter based on the theoretical appraisal of the theoretical situation obtained within the context of nonlocal QCD sum rules and supported by recent high-precision lattice calculations and other experimental data from the pion-photon transition. Though the existing data on the unpolarized

DY $\pi^- N \rightarrow \mu^+ \mu^-$ process cannot single out one particular pion DA with little ambiguity, the “bunch” of the BMS DAs, derived from nonlocal QCD sum rules, seems to comply most favorably with the E615 data. Given the distinctive behavior of all considered pion DAs with respect to the longitudinal momentum fraction, carried by the annihilating quark from the pion in the polarized DY process, one may hope that measuring the angular moment in the planned COMPASS experiment may lend quantitative support for one or the other proposed pion DA.

On the other hand, it is also important to consider another (and actually the most common) mechanism of the $\pi + N$ Drell–Yan process, treating the pion structure in terms of parton distributions rather than the pion DA. This mechanism is the dominant one at moderate values of x_L . There are also related contributions to the SSA due to the imaginary phases emerging in the short-distance subprocesses [32, 33]. These contributions have recently been studied for the kinematics of RHIC and J-PARC [34]. The investigation of the relevance of this mechanism in the case of the COMPASS kinematics requires further investigation.

Acknowledgments

We would like to thank A. V. Efremov and S. V. Mikhailov for discussions and useful remarks. We are grateful to R. Bertini, F. Bradamante, and O. Denisov for discussions on the COMPASS experiment and its potential extension to the Drell–Yan process. Two of us (A.P.B. and O.V.T.) are indebted to Prof. Klaus Goeke for the warm hospitality at Bochum University, where part of this work was carried out. N.G.S. is grateful for support to BLTP@JINR, where this work was completed. O.V.T. is also indebted to M. Anselmino, F. Balestra, R. Bertini, A. Kotzinyan, and G. Pontecorvo for the warm hospitality and useful discussions at INFN (Torino).

This work was supported in part by the Deutsche Forschungsgemeinschaft, grant 436 RUS 113/881/0, the Heisenberg–Landau Programme (grant 2007), the Russian Foundation for Fundamental Research, grants No. 06-02-16215 and No. 07-02-91557, and the Russian Federation Ministry of Education and Science (grant MIREA 2.2.2.2.6546).

-
- [1] S. D. Drell and T.-M. Yan, Phys. Rev. Lett. **25**, 316 (1970).
 - [2] S. Palestini *et al.*, Phys. Rev. Lett. **55**, 2649 (1985).
 - [3] J. S. Conway *et al.*, Phys. Rev. **D39**, 92 (1989).
 - [4] E. L. Berger and S. J. Brodsky, Phys. Rev. Lett. **42**, 940 (1979).
 - [5] A. Brandenburg, S. J. Brodsky, V. V. Khoze, and D. Müller, Phys. Rev. Lett. **73**, 939 (1994).
 - [6] A. Brandenburg, D. Müller, and O. V. Teryaev, Phys. Rev. **D53**, 6180 (1996).
 - [7] R. Bertini, O. Denisov, and S. Paul, Villars Meeting of the CERN SPSC, September 22–28, 2004, Villars, Switzerland; EoI “Drell–Yan program at COMPASS”, COMPASS Collaboration, in preparation.
 - [8] A. P. Bakulev, S. V. Mikhailov, and N. G. Stefanis, Phys. Lett. **B508**, 279 (2001); **B590**, 309(E) (2004).
 - [9] V. L. Chernyak and A. R. Zhitnitsky, Phys. Rept. **112**, 173 (1984).
 - [10] A. V. Efremov and A. V. Radyushkin, Phys. Lett. **B94**, 245 (1980).
 - [11] A. V. Efremov and A. V. Radyushkin, Theor. Math. Phys. **42**, 97 (1980).
 - [12] G. P. Lepage and S. J. Brodsky, Phys. Rev. **D22**, 2157 (1980).

- [13] E. L. Berger, Z. Phys. **C4**, 289 (1980).
- [14] L. Del Debbio, Few Body Syst. **36**, 77 (2005).
- [15] M. Göckeler *et al.*, Nucl. Phys. Proc. Suppl. **161**, 69 (2006), talk in the Workshop on Light-Cone QCD and Nonperturbative Hadron Physics 2005 (LC 2005), Cairns, Queensland, Australia, 7–15 Jul 2005.
- [16] V. M. Braun *et al.*, Phys. Rev. **D74**, 074501 (2006).
- [17] A. P. Bakulev, S. V. Mikhailov, and N. G. Stefanis, Phys. Rev. **D67**, 074012 (2003).
- [18] A. P. Bakulev, S. V. Mikhailov, and N. G. Stefanis, Phys. Lett. **B578**, 91 (2004).
- [19] A. P. Bakulev, S. V. Mikhailov, and N. G. Stefanis, Phys. Rev. **D73**, 056002 (2006).
- [20] J. Gronberg *et al.*, Phys. Rev. **D57**, 33 (1998).
- [21] A. Schmedding and O. Yakovlev, Phys. Rev. **D62**, 116002 (2000).
- [22] A. P. Bakulev, S. V. Mikhailov, and N. G. Stefanis, Annalen Phys. **13**, 629 (2004).
- [23] A. P. Bakulev and A. V. Pimikov, Acta Phys. Polon. **B37**, 3627 (2006).
- [24] K. Hagiwara *et al.*, Phys. Rev. **D66**, 010001 (2002).
- [25] N. G. Stefanis, Nuovo Cim. **A83**, 205 (1984).
- [26] L. Del Debbio, Few Body Syst. **36**, 77 (2005).
- [27] A. P. Bakulev, K. Passek-Kumerički, W. Schroers, and N. G. Stefanis, Phys. Rev. **D70**, 033014 (2004); **D70**, 079906(E) (2004).
- [28] T. Gehrmann and W. J. Stirling, Z. Phys. **C65**, 461 (1995).
- [29] M. Glück, E. Reya, and A. Vogt, Z. Phys. **C67**, 433 (1995).
- [30] C. S. Lam and W.-K. Tung, Phys. Rev. **D21**, 2712 (1980).
- [31] O. V. Teryaev, in *Proceedings of the XI Advanced Research Workshop on High Energy Spin Physics (DUBNA-SPIN-05), September 27–October 1, 2005, Dubna, Russia*, edited by A. V. Efremov and S. V. Goloskokov (JINR, Dubna, 2006), pp. 171–174.
- [32] B. Pire and J. P. Ralston, Phys. Rev. **D28**, 260 (1983).
- [33] R. D. Carlitz and R. S. Willey, Phys. Rev. **D45**, 2323 (1992).
- [34] H. Yokoya, arXiv:0705.2481 [hep-ph].